AIAA JOURNAL
Vol. 43, No. 10, October 2005

Brazier Effect in Multibay Airfoil Sections

Luca S. Cecchini* and Paul M. Weaver†
University of Bristol, Bristol, England BS8 1TR, United Kingdom

Although it has long been recognized that all long thin-walled hollow structures exhibit a nonlinear response to bending moments, the majority of analytical research has focused on circular cross sections. A method of predicting the nonlinear behavior of multibay airfoil sections is presented. Although the approach is simple, the algebraic complexity lends itself toward a solution using algebraic manipulation software. Comparison of the analytical models with finite element analysis shows good correlation and demonstrates the ability of the model in predicting the nonlinear bending response of smooth orthotropic two-bay airfoils.

Nomenclature

$[a]$	=	shell in-plane compliance matrix
C	=	overall curvature
$[D]$	=	shell bending stiffness matrix
E	=	Young's modulus
G	=	shear modulus
h	=	height
I	=	second moment of area
l	=	section Y dimension
M	=	longitudinal bending moment
m	=	cross-sectional bending moment
p	=	cross-sectional reaction force
S	=	wall length
U	=	energy
w	=	cross-section displacement z
α	=	$\cos(\beta)$
β	=	horizontal wall angles to midplane
ε	=	strain
κ	=	cross-sectional curvature
λ	=	element length correction factor
μ	=	I correction factor
ν	=	Poisson's ratio
ψ	=	distributed Brazier crushing force

I. Introduction

IT is well established that long, thin-walled, prismatic sections subject to bending moments suffer a nonlinearity in their bending response. Brazier[1] noted that such structures suffer crushing forces from the rotated (caused by curvature) compressive/tensile forces that arise as a result of bending. These forces reduce the second moment of area of the section and thus its ability to resist bending loads, leading to a nonlinear bending response. In the classic example of a circular, cylindrical tube the structure will ovalize and might eventually crush so much that it is no longer able to sustain the applied bending moment.

The importance of the Brazier effect is not simply its existence as a failure mode, which is generally acknowledged as unlikely to occur (e.g., Corona and Rodrigues[2]). Its significance lies in its contribution to other potential failure modes, namely, local buckling and material failure (through its effect on cross-sectional geometry) as well as its effect on static and dynamic behavior caused by the nonlinearity of the bending response.

Although much work has been carried out on the analysis of circular sections, little has been done on other shapes. The bending of elliptical cross sections, box sections, one- and two-bayed rectangular sections, and initially curved "Fairbairne Crane" type sections have been analytically studied by Huber,[3] Rand,[4] Paulsen and Welo,[5] and Timoshenko,[6] respectively, whereas Mazor and Rand[7] have also developed a numerical method to investigate the behavior of generic hollow cross sections.

It is the aim of this paper to introduce a methodology to provide analytical solutions to predict the nonlinear bending behavior of flapwise symmetric, thin ($h \ll l$), airfoil sections. Because of the lightweight requirements of aircraft design, airfoil sections are typically thin walled and thus highly susceptible to cross-sectional deformations. As such, the calculation of the Brazier deformations is essential in order to provide accurate bending response and accurate local buckling predictions.

The methodology that follows is based on the separation of longitudinal and circumferential effects and the application of distributed loads to the cross section in order to recreate the Brazier crushing forces. The Brazier effect can, of course, be modeled via finite element analysis (FEA); however, the subsequent analytical technique will provide faster solutions and is thus useful in parametric design studies. Furthermore, it can provide a useful insight into the mechanisms involved in the Brazier deformations.

In this paper, subscripts are used to denote sections (letters) and locations (numbers for section intersections, or y); for example, M_{1b} is the local shell bending moment on element b at point 1; 11 and 22 material orientations are longitudinal (spanwise) and circumferential, respectively.

The coordinate system of the cross section (Fig. 1) includes global (Y, Z) and local (y, z) systems. The global coordinate system has its origin at the neutral axis, whereas local systems originate at the left-most corner for horizontal elements and at the neutral axis for vertical elements. The X axis points spanwise along the blade.

To simplify the subsequent expressions, α is introduced such that

$$\alpha_n = \cos\beta_n$$

giving, for example,

$$S_a = l_a/\alpha_a$$

II. Analysis

Airfoil sections are complex structures: curved, multibayed, and potentially of variable composite material construction, with a typical profile shown in Fig. 2. To simplify the analysis, each bay's cross section is initially modeled as a series of straight elements of orthotropic material. A method to account for smooth surfaces will be demonstrated later. Only two bayed structures are examined in this paper, but the method is applicable to any number of bays.

Presented as Paper 2004-1522 at the AIAA/ASME/ASCE/AHS/ASC 45th Structures, Structural Dynamics, and Materials Conference, Palm Springs, CA, 19–22 April 2004; received 4 August 2004; revision received 16 March 2005; accepted for publication 2 April 2005.

*Ph.D. Student, Department of Aerospace Engineering, Queen's Building; luca.cecchini@bristol.ac.uk. Student Member AIAA.

†Senior Lecturer, Department of Aerospace Engineering, Queen's Building; paul.weaver@bristol.ac.uk. Member AIAA.

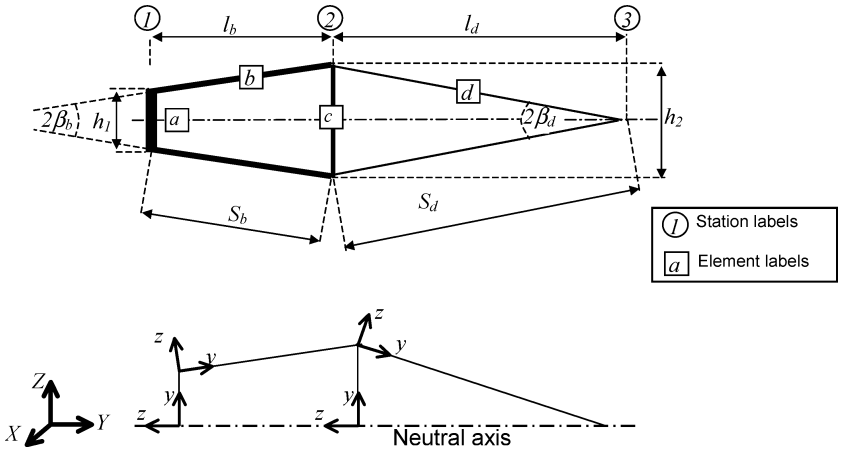

Fig. 1 Cross-section nomenclature and coordinate system.

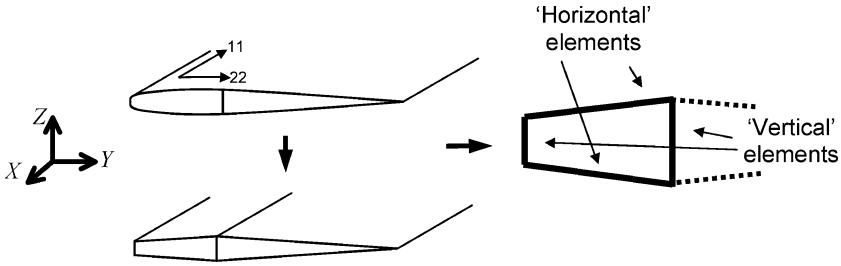

Fig. 2 Typical rotor cross section and simplified "box" idealization.

In a similar manner to Brazier's analysis, the approach is energy based and separates longitudinal and cross-sectional effects; however, rather than finding the cross-sectional deformation mode by the calculus of variations, a distributed crushing force is applied to the cross-section. The cross section is decomposed into two types of straight element, "vertical" and "horizontal" (Fig. 2), and these are discussed individually. The analysis is dependent on symmetry around the flapwise axis, and therefore only one half of the structure is modeled.

A. Horizontal Elements

Brazier crushing forces arise from rotated (through bending curvature) longitudinal stresses, generating a component through the cross section. These longitudinal X stresses are directly proportional to local in-plane stiffness $1/a_{11}$ and the local strain, which is proportional to the distance from the neutral axis and the section curvature caused by deflection. Because the undeformed distance to the neutral axis of any point y along element b or d is given by

$$Z_b = (h_2/2)[h_1/h_2 + (y/S_b)(1 - h_1/h_2)] \tag{1a}$$

$$Z_d = (h_2/2)[1 - y/S_d] \tag{1b}$$

the initial, local crushing force (ψ_{yb}) along elements b and d, per unit length dy, is given by

$$\psi_{yb} = \psi_{\max(b)}[h_1/h_2 + (y/S_b)(1 - h_1/h_2)]\,\mathrm{d}y \tag{2a}$$

$$\psi_{yd} = \psi_{\max(d)}[1 - y/S_d]\,\mathrm{d}y \tag{2b}$$

where $\psi_{\max(\,)}$ is the instantaneous maximum crushing force per unit length of the element. Equations (2a) and (2b) distribute the Brazier load based upon the undeformed geometry of the cross section; however, as the section deforms the actual local proximity to the neutral axis will vary from Eqs. (1a) and (1b). To compensate for this, although the crushing force distribution is based upon the undeformed geometry, the maximum crushing force $\psi_{\max(b)}$ remains unknown and is calculated by minimization of the energy of the system (see Sec. II.C).

It is assumed that the crushing force is generated solely by the horizontal elements, whereas the vertical elements only resist this force and its associated bending moments. This assumption is reasonable for slender rotor sections, where the crushing moment contribution of the vertical elements will be relatively small. Furthermore, any such crushing force will principally be resisted by direct strains in the vertical element (discussed later) and will not affect the horizontal elements.

The loads in Eqs. (2a) and (2b) are therefore applied to the horizontal elements as distributed loads on two-dimensional beams (Fig. 3a). All internal forces on the elements are maintained as positive in the y direction and clockwise for simple interfacing with other elements. This might, however, result in negative reaction forces indicating reactions in the opposite direction to the arrows. Force p_{yb} represents the shear force acting on the face of an elemental segment dy along section b.

In Fig. 3, y' is the distance of an elemental piece of section b, of length dy', between 1 and y. Assuming that the shells are circumferentially incompressible, and only react loads by bending (a valid assumption for thin-walled airfoils, where shear deformation will be relatively small), the forces acting around a point y along an element can be found (Fig. 3b) and resolved perpendicular to the shell walls (Fig. 3c). From static equilibrium considerations, resolving section b's forces gives

$$\begin{aligned} p_{1b}\alpha_b &= -p_{2b}\alpha_b + \alpha_b \int_0^{S_b} \psi_{yb}\,\mathrm{d}y \\ &= -p_{2b}\alpha_b + \frac{1}{2}\psi_{\max(b)} S_b \alpha_b \left[1 + \frac{h_1}{h_2}\right] \end{aligned} \tag{3a}$$

$$\begin{aligned} m_{1b} &= -m_{2b} - p_{2b} S_b \alpha_b + \alpha_b \int_0^{S_b} \psi_{yb}\, y\,\mathrm{d}y \\ &= -m_{2b} - p_{2b} S_b \alpha_b + \frac{1}{6}\psi_{\max(b)} \alpha_b S_b^2 \left[2 + \frac{h_1}{h_2}\right] \end{aligned} \tag{3b}$$

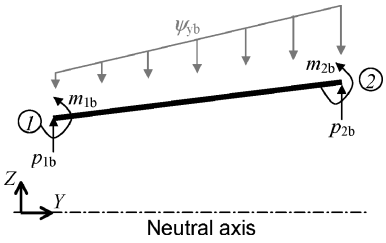

a) Force distribution

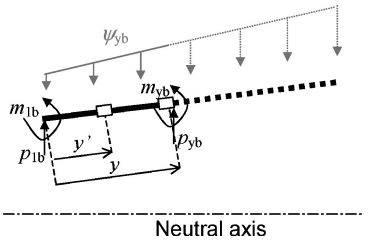

b) Forces around arbitrary point

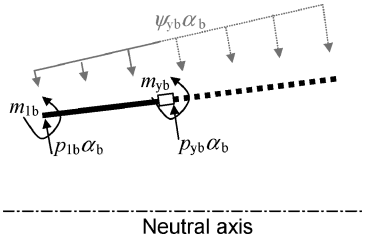

c) Resolved forces around arbitrary point

Fig. 3 Force distributions around element *b*.

$$m_{yb} = -m_{1b} + p_{1b} y \alpha_b - \alpha_b \int_0^y \psi_{y'b}[y - y']\,\mathrm{d}y'$$
$$= -m_{1b} + p_{1b} y \alpha_b - \frac{1}{6}\psi_{\max(b)} \alpha_b y^2 \left[3\frac{h_1}{h_2} + \frac{y}{S_b}\left(1 - \frac{h_1}{h_2}\right)\right] \quad (3c)$$

and section d's as

$$p_{2d}\alpha_d = -p_{3d}\alpha_d + \alpha_d \int_0^{S_d} \psi_{yd}\,\mathrm{d}y$$
$$= -p_{2d}\alpha_d + \frac{1}{2}\psi_{\max(d)} S_d \alpha_d \quad (4a)$$

$$m_{2d} = -m_{3d} - p_{3d} S_d \alpha_d + \alpha_d \int_0^{S_d} \psi_{yd}\, y\,\mathrm{d}y$$
$$= -m_{3d} - p_{3d} S_d \alpha_d + \frac{1}{6}\psi_{\max(d)} \alpha_d S_d^2 \quad (4b)$$

$$m_{yd} = -m_{2d} + p_{2d} y \alpha_d - \alpha_d \int_0^y \psi_{y'd}[y - y']\,\mathrm{d}y'$$
$$= -m_{2d} + p_{2d} y \alpha_d - \frac{1}{6}\psi_{\max(d)} \alpha_d y^2 \left[3 - \frac{y}{S_d}\right] \quad (4c)$$

Thus the local curvature of the b element is given by

$$\kappa_{yb} = \left.\frac{\mathrm{d}^2 w}{\mathrm{d}y^2}\right|_b = \frac{m_{yb}}{D_{22(b)}} \quad (5)$$

where w is the displacement perpendicular to b. The change in local gradient is the integral of the curvature

$$\left.\frac{\mathrm{d}w}{\mathrm{d}y}\right|_{yb} = \int \frac{m_{yb}}{D_{22(b)}}\,\mathrm{d}y + \left.\frac{\mathrm{d}w}{\mathrm{d}y}\right|_{1b} \quad (6)$$

where $\mathrm{d}w/\mathrm{d}y|_{1b}$ is the change in gradient of the horizontal element at point 1 ($y = 0$). Therefore at 2 ($y = S_b$),

$$\left.\frac{\mathrm{d}w}{\mathrm{d}y}\right|_{2b} = \frac{1}{D_{22(b)}}\left[\begin{array}{c} -m_{1b} S_b + \frac{1}{2} p_{1b}\alpha_b S_b^2 \\ -\frac{1}{24}\alpha_b S_b^3 \psi_{\max(b)}\left(1 + 3\frac{h_1}{h_2}\right)\end{array}\right] + \left.\frac{\mathrm{d}w}{\mathrm{d}y}\right|_{1b} \quad (7)$$

Integration gives the displacement of the horizontal element as

$$w_{yb} = \iint \frac{m_{yb}}{D_{22(b)}}\,\mathrm{d}y\,\mathrm{d}y + \left.\frac{\mathrm{d}w}{\mathrm{d}y}\right|_{1b} y + w_{1b} \quad (8)$$

and therefore the displacement at 2 is given by

$$w_{2b} = \frac{1}{D_{22(b)}}\left[\begin{array}{c} -\frac{1}{2} m_{1b} S_b^2 + \frac{1}{6} p_{1b}\alpha_b S_b^3 \\ -\frac{1}{120}\psi_{\max(b)}\alpha_b S_b^4\left(1 + 4\frac{h_1}{h_2}\right)\end{array}\right] + \left.\frac{\mathrm{d}w}{\mathrm{d}y}\right|_{1b} S_b + w_{1b} \quad (9)$$

The energy of cross-sectional deformation of two elements (one above, one below the neutral axis) is given by

$$U_{\mathrm{circ}(a)} = 2\frac{1}{2}\int_0^{S_b} \kappa_{yb}^2 D_{22(b)}\,\mathrm{d}y = \frac{1}{D_{22(b)}}\int_0^{S_b} m_{yb}^2\,\mathrm{d}y \quad (10)$$

where m_{yb} is found from Eq. (3c). If $D_{11(b)}$ contribution to longitudinal stiffness is considered negligible, in accordance with thin-walled, semimembrane, assumptions, the contribution of an element $\mathrm{d}y$ to the longitudinal bending stiffness is given by the square of its deformed distance to the neutral axis [Eq. (1a) plus Z displacement], multiplied by the longitudinal in-plane stiffness $1/a_{11}$. Thus the longitudinal bending stiffness from the b section is given by

$$EI_b = 2\frac{1}{a_{11(b)}}\int_0^{S_b} [Z_b + w_{yb}\alpha_b]^2\,\mathrm{d}y$$
$$= 2\frac{1}{a_{11(b)}}\int_0^{S_b}\left[\frac{h_1}{2} + \frac{y}{2S_b}(h_2 - h_1) + w_{yb}\alpha_b\right]^2\mathrm{d}y \quad (11)$$

The EI term is also doubled to take into account the corresponding, identical, element beneath the neutral axis. Thus the energy of longitudinal bending is given by

$$U_{b(\mathrm{long})} = \frac{1}{2} EI_b C^2$$
$$= C^2\frac{1}{a_{11(b)}}\int_0^{S_b}\left[\frac{h_1}{2} + \frac{y}{2S_b}(h_2 - h_1) + w_{yb}\alpha_b\right]^2\mathrm{d}y \quad (12)$$

The equivalent analyses must be repeated for section d.

B. Vertical Elements

As already stated, it is assumed, in this analysis, that the vertical sections are not themselves subjected to any Brazier loading, but only react to the forces from the horizontal sections (Fig. 4).

As drawn in Fig. 4, forces p_{ya} and p_{1a} will be equal, but with opposite signs, as will moments m_{ya} and m_{1a}. In the original, undeformed, configuration, the force p_{1a} will not produce a bending moment on the vertical element as it acts along the same vector as p_{ya}. As the vertical elements deform, however, a bending moment caused by p_{1a} around y will be generated, as a relative z displacement manifests itself between 1 and y. Because the analysis is restricted to slender structures ($h/l \ll 1$) and small displacements, lateral deflection can be assumed to be small, removing this effect and greatly simplifying the analysis. Thus if the deflection of the

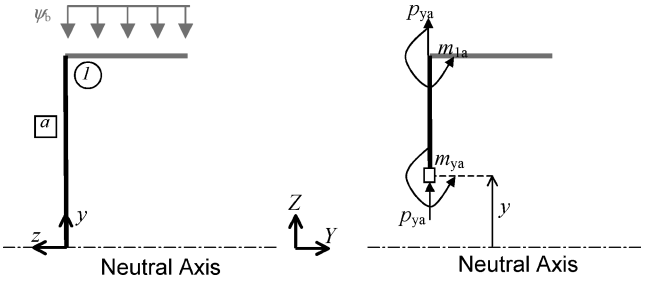

Fig. 4 Element *a* force nomenclature.

vertical wall is entirely caused by the end moments,

$$\kappa_a = \left.\frac{\mathrm{d}^2 w}{\mathrm{d}y^2}\right|_a = \frac{m_{1a}}{D_{22a}} \tag{13}$$

producing a single, constant, radius of curvature. Because of symmetry around the neutral axis, rotation at $y = 0$ is zero, and the rotation of element a at 1 ($y = h_1/2$) is given by

$$\left.\frac{\mathrm{d}w}{\mathrm{d}y}\right|_{1a} = \int_0^{h_1/2} \kappa_a \,\mathrm{d}y = \frac{\kappa_a h_1}{2}$$

which rearranges to

$$\kappa_a = \left.\frac{2}{h_1}\frac{\mathrm{d}w}{\mathrm{d}y}\right|_{1a} \tag{14}$$

The shortening of the vertical wall is often overlooked in analyses of this type.[5,6] This can be a shortcoming because it is critical to the onset of limit moments in structures with large h/l or where the vertical walls have a significantly lower D_{22} than the horizontal sections, but in thin airfoil sections these effects can safely be ignored. The inclusion of vertical shortening and the offset vertical loads would lead to a prediction of the buckling behavior of the vertical element (because of the negative p_{1a}), a phenomenon that is not considered here for the aforementioned reasons. The energy of deforming each vertical section is given by

$$U_{\mathrm{circ}(a)} = 2\int_0^{h_1/2} \frac{1}{2}\kappa_a^2 D_{22(a)}\,\mathrm{d}y = \frac{2}{h_1}\left(\left.\frac{\mathrm{d}w}{\mathrm{d}y}\right|_{1a}\right)^2 D_{22(a)} \tag{15}$$

With vertical element shortening assumed to be small, the longitudinal bending stiffness is constant

$$EI_a = h_1^3 \big/ 12a_{11(a)} \tag{16}$$

and the energy of longitudinal deformation is given by

$$U_{\mathrm{long}(a)} = (1/24)C^2\left(h_1^3 \big/ a_{11(a)}\right) \tag{17}$$

All of these equations must be reproduced for section c.

C. Overall Behavior

By assuming no shortening of the vertical walls

$$w_{1b}\alpha_b = w_{2b}\alpha_b = w_{2d}\alpha_d = w_{3d}\alpha_d = 0$$

and by linking rotations

$$\left.\frac{\mathrm{d}w}{\mathrm{d}y}\right|_{1a} = \left.\frac{\mathrm{d}w}{\mathrm{d}y}\right|_{1b}, \qquad \left.\frac{\mathrm{d}w}{\mathrm{d}y}\right|_{2b} = \left.\frac{\mathrm{d}w}{\mathrm{d}y}\right|_{2c} = \left.\frac{\mathrm{d}w}{\mathrm{d}y}\right|_{2d}, \qquad \left.\frac{\mathrm{d}w}{\mathrm{d}y}\right|_{3d} = 0$$

and moments

$$m_{1a} + m_{1b} = 0, \qquad m_{2c} + m_{2d} + m_{2b} = 0$$

at the interfaces and substitution into the energy terms [Eqs. (10), (12), (15), and (17)], all except two unknowns can be eliminated. The actual identity of the unknown parameters is not important for these sections, but for the purpose of this analysis it was left as the two distributed Brazier crushing forces ($\psi_{\max(b)}$ and $\psi_{\max(d)}$). The total energy of the system can then be expressed as

$$U_{\mathrm{tot}} = \sum_{n=a\to d}\left(U_{\mathrm{circ}(n)} + U_{\mathrm{long}(n)}\right) \tag{18}$$

which can be differentiated with respect to both $\psi_{\max(b)}$ and $\psi_{\max(d)}$ (which are independent of each other) and equated to zero, leading to the minimum-energy solution for both parameters:

$$\frac{\partial U_{\mathrm{tot}}}{\partial \psi_{\max(d)}} = \frac{\partial U_{\mathrm{tot}}}{\partial \psi_{\max(d)}} = 0$$

These expressions can then be substituted back into the longitudinal stiffness equations, and the longitudinal bending moment/curvature response can be found from Eqs. (11) and (16) as

$$M_{\mathrm{tot}} = \sum_{n=a\to d}(M_n)$$

$$= C\left[\frac{h_1^3}{12a_{11(a)}} + 2\frac{1}{a_{11(b)}}\int_0^{S_b}\left(\frac{h_1}{2} + \frac{y}{2S_b}[h_2 - h_1] + \alpha_b w_{yb}\right)^2 \mathrm{d}y + \frac{h_2^3}{12a_{11(c)}} + 2\frac{1}{a_{11(d)}}\int_0^{S_d}\left(\frac{h_2}{2}\left[1 - \frac{y}{S_d}\right] + \alpha_d w_{yd}\right)^2 \mathrm{d}y\right] \tag{19}$$

Because of the complexity of the equations, principally as a result of the squaring of the terms inside the integral in Eq. (12) (and its equivalent for the trailing edge), the analysis is best carried out using algebraic manipulation software (e.g., MAPLE[8]). Figures 5a and 5b compare finite element analysis (FEA; see Appendix) with analytical solutions for two sections of homogeneous aluminum (Table 1) plate construction (1 mm thick on all sides), with principal dimensions as given. The material is assumed to remain elastic through the entire response in both FEA and analytical modeling, and thus the finite element analysis is used to verify the analytical techniques and provide confidence in the analytical methods.

The more slender section's analytical solution follows the FEA solution very well (Fig. 5b), whereas that of the deeper section shows errors at higher deformations not capturing the collapse moment. These inaccuracies principally arise as a result of the approximate modeling of the vertical sections and in particular the assumption that they do not shorten as a result of curvature (which assumes $h/l \ll 1$, not the case for the deep section). A further, albeit smaller, source of error at large deformations is the assumption that the Brazier crushing force remains linearly distributed, as per Eq. (2). As the section crushes, the walls no longer remain straight, changing the crushing force distribution and resulting in an inaccurate representation of the deformation of the element.

The dashed line in Fig. 5 represents the approximate longitudinal material failure point (0.6% strain). The estimate is somewhat conservative, as it assumes that the maximum height of the section remains the same, whereas in reality Brazier-induced flattening will reduce the maximum distance to the neutral axis, thus reducing maximum longitudinal strains. Neither local buckling nor circumferential material failure modes are considered here.

Table 1 Aluminum material properties

Property	Value
Young's modulus E, GPa	70
Poisson's ratio ν	0.3
Shear modulus G, GPa	27
Failure strain $\varepsilon_{\max}$, %	0.6
Wall thickness, mm	1

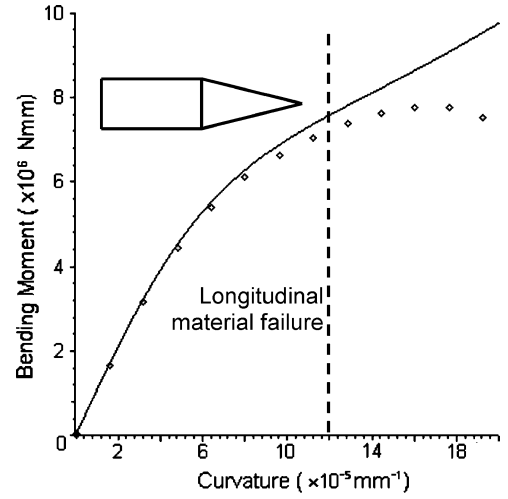

a) $l_b = l_d = 200$ **mm,** $h_1 = h_2 = 100$ **mm**

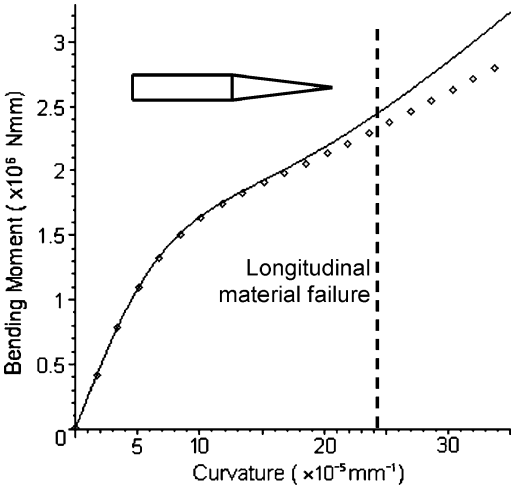

b) $l_b = l_d = 200$ **mm,** $h_1 = h_2 = 50$ **mm**

Fig. 5 Straight section bending moment response plots: · · · ·, FEA and ——, analytical.

D. Curved Sections

Modeling has so far been limited to straight box-type sections; however, real airfoil sections have rounded shapes for smooth airflow (with the rather limited exception of early stealth aircraft). Thus a method of analyzing such structures would be useful, but a full solution of the preceding equations including curvature terms is complicated. Two separate methods are used here to deal with such sections, and they can be applied individually or simultaneously to the analysis of structures.

1. Correction Factors

The simplest method of accounting for curvature is simply to add geometric correction factors to the section. This approach assumes that for small initial surface curvatures the deformation mechanism remains the same as if it were straight. The circumferential energy equations are multiplied by the ratio of perimeter lengths of the real section relative to the box model, to compensate for the increased amount of material undergoing deformation. The longitudinal stiffnesses are multiplied by the ratio of initial second moment of area between the box and the real section. Thus Eq. (18) becomes

$$U_{\text{tot}} = \sum_{n=a\to d} \left(\lambda_n U_{\text{circ}(n)} + \mu_n U_{\text{long}(n)}\right) \tag{20}$$

while Eq. (19) becomes

$$M_{\text{tot}} = \sum_{n=a\to d} (\mu_n M_n) \tag{21}$$

where

$$\lambda = S_{\text{actual}}/S_{\text{flat}}, \qquad \mu = I_{\text{actual}}/I_{\text{flat}}$$

In these equations S_{actual} and I_{actual} are the real initial element lengths and second moments of area (extracted from geometrical data), and S_{flat} and I_{flat} are their equivalents in the box representation. However, depending on how the blade section is represented using the elements, it might not be obvious exactly where to apply individual correction factors (particularly with the use of multiple elements, as stated next), and hence global factors might be more appropriate (for example a single λ and μ for the whole cross section, or for each bay).

2. Multielement Construction

A further method of dealing with curved surfaces is to construct them out of a series of interconnected horizontal elements (Fig. 6).

By attaching a series of horizontal sections together, a better representation of the undeformed geometry can be obtained. Each additional section, however, introduces a new series of unknowns and boundary conditions. Using the nomenclature in Fig. 7, for the nose bay (noting that it has changed from Fig. 1 to accommodate the extra elements) the displacement boundary conditions at the joined horizontal elements (station 2) can be found.

To ensure compatibility, rotations are matched with neighboring elements to give

$$\left.\frac{\mathrm{d}w}{\mathrm{d}y}\right|_{2b} = \left.\frac{\mathrm{d}w}{\mathrm{d}y}\right|_{2d}$$

matching translations, but recalling they are not necessarily zero gives

$$w_{2b}\alpha_b = w_{2d}\alpha_d$$

and because at element interfaces forces must sum to zero,

$$m_{2b} + m_{2d} = 0, \qquad p_{2b} + p_{2d} = 0$$

These can once again be substituted into the energy terms [Eqs. (10), (12), (15), and (17)] and used to eliminate all except two unknowns (one per horizontal element). The rest of the calculation remains identical to that for sections with only a single element per bay, with the minimization of energy with respect to these new unknowns and calculation of overall bending moment. The introduction of these extra elements does add to the complexity of the solution, and, although in principle any number of elements can be strung together to improve the solution accuracy, excess elements can cause solution problems for algebraic manipulation software.

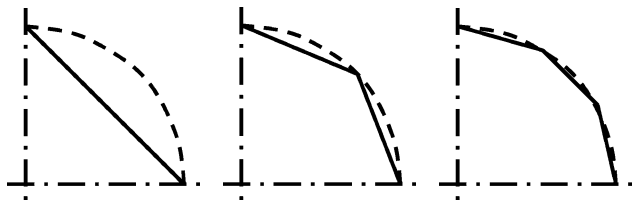

a) One section **b) Two sections** **c) Three sections**

Fig. 6 Curved section representations with interconnected horizontal elements.

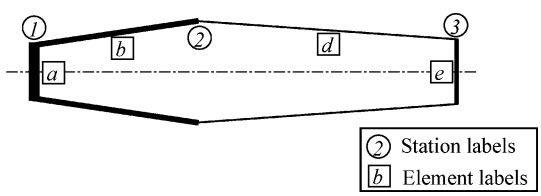

Fig. 7 Multielement section labeling.

3. Example

A NACA0012 profile, divided into two bays through the midchord, was used as an example to demonstrate the efficacy of the methods to represent curved structures. Figure 8 shows the NACA0012 profile with a vertical spar at half-chord and the approximate box models used to represent it. The multielement model has two horizontal elements in the leading edge, but because of the low trailing-edge curvature only one element in the tail. The total length of the single nose-element model is slightly shorter than the full length of the blade, because the construction of the blade with elements is an approximate process.

For this test a very thin-walled (1 mm thick, all-round, for a 500-mm chord length), aluminum wing was analyzed using FEA and the aforementioned analysis technique. The results are shown in Fig. 9 (material and blade data shown in Tables 1–5). It is apparent from Fig. 9a that the response of the uncorrected single element analytical model does not follow that of the FEA. This is, in large part, caused by the straight nose element being, on average, much closer to the neutral axis than in the real section, significantly reducing the initial second moment of area. With the application of the geometrical correction factors [Eqs. (20) and (21)], this response is much improved, despite solution errors at large deformations, with the plateau load accurately predicted. The introduction of an extra nose element (Fig. 8c) brings further improvement, minimizing the need for correction factors, by accurately predicting initial stiffness. Furthermore, the extra element significantly improves large curvature response prediction (beyond the plateau load; Fig. 9b).

A composite blade (of the same cross-sectional geometry) was also tested to demonstrate the validity of the method with orthotropic shells. Three different carbon-fiber-reinforced plastic (CFRP) lay ups were used around the section, as noted in the Table 6, and this analysis was only carried out using the multielement model with correction factors. Once again good correlation was found between FEA and analytical results (Fig. 10), solution divergence occurring only once the tail element has crushed such that the trailing-edge elements come into contact (dotted line in Fig. 10). At this load neither FEA nor analytical accurately predict behavior caused by the lack of contact elements in the FEA model (Appendix).

In these examples material failure from longitudinal strains (matrix failure at $C \approx 1.7 \times 10^{-6}$ mm^{-1}) does not preempt the occurrence of large deformation effects. Local buckling and circumferential material failure are not examined here, but considering the

Table 2 CFRP material properties

Property	Value
E_{11}, GPa	140
E_{22}, GPa	10
ν_{12}	0.3
G_{12}, GPa	5
Failure strain $\varepsilon_{11\,\max}$, %	0.9%
Failure strain $\varepsilon_{22\,\max}$, %	0.5%
Lamina thickness, mm	0.25

Table 3 Blade cross section

Property	Value
Blade profile	NACA0012
Chord length, mm	500
Max height, mm	60
Midwall to nose, mm	250
Midwall height, mm	49.1

Table 4 Single-element blade model properties

Property	Value
l_b, mm	237.8
l_d, mm	250
h_1, mm	25.9
h_2, mm	49.1
λ_a	1.438
λ_b	1.001
λ_d	1
μ_a	1.747
μ_b	1.917
μ_d	1.027

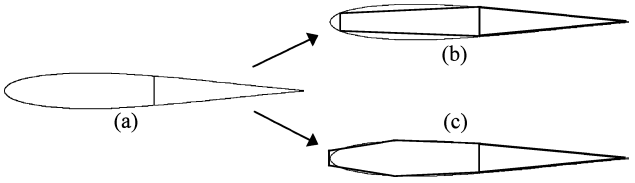

Fig. 8 NACA0012 a) wing, b) normal approximation, and c) multielement approximation.

Table 5 Multielement blade model properties

Property	Value
l_b, mm	82.7
l_d, mm	167.3
l_f[a], mm	250
h_1, mm	33.4
h_2, mm	54.7
h_3, mm	49.1
$\lambda_{a,b,d}$, mm	1.030
λ_f[a]	1.028
$\mu_{a,b,d}$	1.081
μ_f[a]	1

[a] f is the trailing-edge horizontal element.

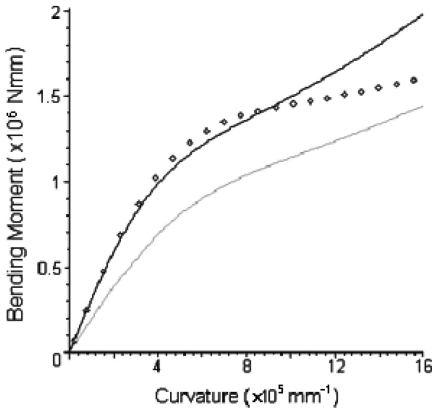

a) Single-element nose

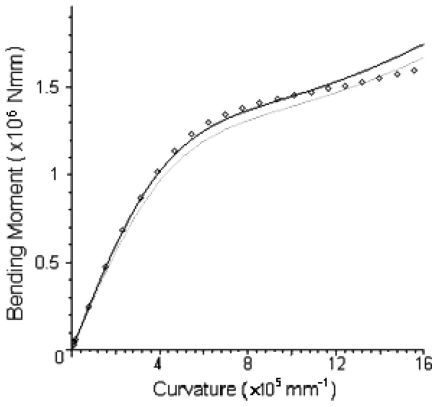

b) Double-element nose

Fig. 9 Aluminum NACA0012 bending response: · · · ·, FEA; ——, corrected analytical; and gray line, uncorrected analytical.

Table 6 Composite blade lay up

Element	Lay up
Nose skin	$[0,90,0,0]_s$
Midwall	$[90,90,0,0]_s$
Tail skin	[0,90,0]

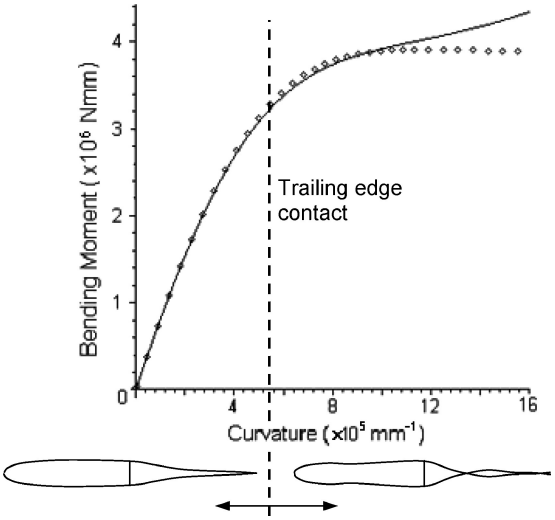

Fig. 10 CFRP NACA0012 bending response: · · · ·, FEA and ——, corrected analytical.

thin nature of the shell the former is likely to be worthy of particular consideration, almost certainly occurring before the plateau load, and must be analyzed with Brazier deformations taken into consideration.

III. Conclusions

A method for the analysis of the Brazier response of two-bay airfoil sections is presented. The accuracy of the model is sufficient to give a good first indication of initial nonlinear response of an airfoil, for significantly less computational time than finite element analysis. Although the solution is closed form, the complexity of the equations requires their solution using algebraic manipulation software.

Appendix: Finite Element Modeling

To test the validity of the analytical models, bending moment/deflection comparisons were carried out for the various sections with finite element (FE) models. The FE analysis was carried out using the HKS Abaqus/Standard[9] package using the technique specified in the Abaqus Benchmarks Manual.[10] The FE models were constructed of S8R, eight-noded, reduced integration, quadratic shell elements, in order to allow accurate curvature description. The models were of single-element extruded depth (in the X direction), with symmetry boundary conditions on one face and a planar rotation (with in-plane freedom of displacement) imposed on the other face via the Abaqus *SURFACE command. As such, all nodes on the face were constrained to remain attached and perpendicular to a plane that was subsequently rotated to generate the longitudinal curvature. The solution, through necessity, was carried out using geometrically

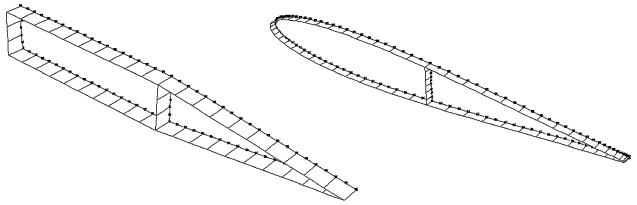

Fig. A1 Box and NACA0012 airfoil FE models.

nonlinear static analysis, the Brazier crushing force arising from the rotated reaction forces on the symmetry and the rotated planes.

The FE meshes are shown in Fig. A1, where the dots, attached to one face of each structure, represent the nodes on the rotated surface. In the NACA0012 model, the trailing edge is closed at the tip via a single vertical element.

The extrusion of the section is kept small in order to prevent the occurrence of local buckling, as it was desired to observe the entire nonlinear response curve caused solely by Brazier effects. In keeping with this, material was assumed to be entirely elastic, and thus material plasticity nonlinearities were avoided.

Contact surfaces, to prevent elements passing through each other, were not specified in the FE models. Thus for large cross-sectional deformations (Fig. 10), behavior is not accurately predicted.

Acknowledgments

The authors thank AgustaWestland Helicopters and the Engineering and Physical Sciences Research Council for their contributions to this research. We also thank Graham Hill for his assistance with the finite element modeling, Neil Taylor and James Rodgers for their assistance with wing profiles, and Ian Farrow for his assistance on geometry.

References

[1]Brazier, L. G., "The Flexure of Thin Cylindrical Shells and Other 'Thin' Sections," *Late of the Royal Aircraft Establishment*. Repts. and Memoranda, No. 1081 (M.49.), Royal Aircraft Establishment, Farnborough, England, U.K., 1926, pp. 1–30.

[2]Corona, E., and Rodrigues, A., "Bending of Long Cross-Ply Composite Cylinders," *Composites Engineering,* Vol. 5, No. 2, 1995, pp. 163–182.

[3]Huber, M. T., "The Bending of Curved Tube of Elliptic Sections," *Proceedings of the Seventh International Congress for Applied Mechanics*, Vol. 1, edited by H. Levy, Her Majesty's Stationery Office, London, 1948, pp. 322–328.

[4]Rand, O., "In-Plane Warping Effects in Thin-Walled Box Beams," *AIAA Journal*, Vol. 38, No, 3, 2000, pp. 542–544.

[5]Paulsen, F., and Welo, T., "Cross-Sectional Deformations of Rectangular Hollow Sections in Bending: Part II, Analytical Models," *International Journal of Mechanical Sciences*, Vol. 43, No. 1, 2001, pp. 131–152.

[6]Timoshenko, S., "Bending Stresses in Curved Tubes of Rectangular Cross-Section," *Transactions of the American Society of Mechanical Engineers*, Vol. 45, May 1923, pp. 135–140.

[7]Mazor, D., and Rand, O., "The Influence of the in-Plane Warping on the Behavior of Thin-Walled Beams," *Thin-Walled Structures*, Vol. 37, No. 4, 2000, pp. 363–390.

[8]MAPLE, Algebraic Manipulations Software Package, ver 8.00, Waterloo Maple, Inc., Waterloo, ON, Canada, 2002.

[9]Abaqus/Standard, Finite Element Analysis Software Package, ver 6.2, Hibbitt, Karlsson and Sorensen, Providence, RI, 2001.

[10]Abaqus Benchmarks Manual, ver. 6.2, Hibbitt, Karlsson and Sorensen, Providence, RI, 2001, Sec. 1.1.5.

B. Sankar
Associate Editor